

Analysis of Failure Causes of 0Cr19Ni9 Blade Crack

Xiaopeng LI¹, Renheng HAN¹, Youshui XIE¹, Yan LI¹, Yalong GAO²,
Xiaoming WANG², Qiuju ZHU², Hexin ZHANG^{1*}, Chengzhi ZHAO^{1,2}

¹ College of Materials Science and Chemical Engineering, Harbin Engineering University, No. 145 Nantong Avenue, Harbin, Heilongjiang, 150001, China

² Harbin Xinrun Industry Co., Ltd. No. 6 Pingling Road, Harbin, Heilongjiang, 150300, China

crossref <http://dx.doi.org/10.5755/j02.ms.29877>

Received 24 September 2021; accepted 06 December 2021

In this paper, fracture morphology observation, microstructure analysis, standard corrosion test, and other experimental methods are used to analyze the causes of corrosion and cracking of steam turbine blades (0Cr19Ni9) produced by a certain company. The results showed that cracks appeared during the operation of the blade. A large number of dimples were observed under the scanning electron microscope, almost all of which were shear dimples; at the same time, fatigue bands were also distributed in them. The internal cause of the cracks is the long-term service, which causes the carbon and the alloy to undergo a diffusion reaction to form carbon-rich areas and carbides. They are thermally corroded in the service environment, and the carbon-rich zone is reduced, which reduces the strength of the zone; carbides accumulate at the grain boundary, causing groove-shaped defects at the grain boundary to form a cutting effect. It is easy to form a source of fatigue cracks. The external cause is that the material is subjected to transverse stress for a long time during operation, which leads to the generation of cracks. This article analyzes the failure causes of the blade and proposes related solutions, which have important reference value for production practice.

Keywords: corrosion cracking, intergranular corrosion, Cr₂₃C₆, blades.

1. INTRODUCTION

A power station steam turbine is an important power device in a power station. As an important part of the power station steam turbine, the performance requirements of the blades are extremely harsh in the working environment of high temperature and high pressure for a long time [1–3]. Due to the high operating temperature, pressure, impact, and corrosion, the causes of blade failure are more complicated. Generally, blades are used for a long time, and blades are at the core of power station steam turbines, so the importance of research on blade failure problems can be seen.

The blade (0Cr19Ni9) produced by a company was damaged at 537 °C and 17.5 MPa in the working environment after 27600 h of operation. After inspection, it was found that cracks and failures occurred at the root of the blade. At present, what is the main cause of damage to the blade? What are the conditions for maintenance or replacement? In response to these problems, due to the lack of experimental data, only experience can be used as a guide [4]. To explore the causes of failure, extend the life of the equipment, ensure safe production, and provide a scientific basis for equipment maintenance, it is necessary to study the failure of the blade.

In this paper, fracture morphology observation, microstructure morphology analysis, standard corrosion test, and other experimental methods are used to analyse the crack failure of the blade (0Cr19Ni9). The main reasons for the cracks of the blade (0Cr19Ni9) are analyzed from the internal and external factors, and corresponding measures are proposed to improve the service life of the blade.

2. EXPERIMENTAL MATERIALS AND EXPERIMENTAL PROGRAMS

2.1. Experimental materials

The material used in this study is a coil made of 0Cr19Ni9 thin plate scrap of the same grade. During smelting, it is prepared by pre-furnace analysis and supplemented with low-content elements. The molten steel is melted in ZG-0.05LB induction furnace, poured in a plum blossom sample mold, and cooled in the atmosphere. After the smelting is completed, the plum blossom samples are processed into tensile samples and small pieces of flakes. The chemical composition of 0Cr19Ni9 steel was analysed by M5000 direct reading spectrometer. The chemical composition of 0Cr19Ni9 is shown in Table 1. The material contains a large amount of Cr and Ni. Cr and Ni are austenite stabilizing elements, so the matrix of the material is austenite [5, 6]. Put the sample into the HVAF-240 heat treatment furnace for the experiment. The heat treatment process is as follows: After heating to 1050 °C with the furnace, solid solution for 2 h, then take out the sample and cool it to room temperature in air.

2.2. Experimental program

2.2.1. Tensile test

Use 1500 # sandpaper to polish the surface of the tensile sample to prevent stress concentration in scratches and line cutting marks, which will affect the tensile results.

* Corresponding author. Tel.: +86 18645106806
E-mail address: zhanghx@hrbeu.edu.cn (H. Zhang)

Table 1. Chemical composition analysis of 0Cr19Ni9 test steel (wt.%)

Element	C	Si	Mn	Cr	Ni	Fe
Content	0.054	0.652	1.115	19.19	9.03	Bal.
Required	≤ 0.08	≤ 1.00	≤ 2.00	17.00 ~ 20.00	8.00 ~ 10.50	Bal.

The tensile sample is tested on the Instron 5599 electronic universal testing machine, and the tensile rate is 1×10^{-3} mm/min. After the stretching is completed, the fracture morphology is observed on the macroscopic morphology, and the microscopic morphology is observed by the JEOL-6380LV scanning electron microscope (SEM).

2.2.2. Intergranular corrosion standard test

This paper uses the GB/T 4334-2008 intergranular corrosion standard test to detect whether the material has an intergranular corrosion tendency [7]. The experimental method is as follows: (1) Grind and polish the surface of the divided small sample, with a 65 wt.% nitric acid alcohol solution. Put the processed sample into a 1L conical flask with a reflux condenser, pour the prepared nitric acid solution, and put it into the oil bath of the C-MAG HS7 magnetic stirrer. Adjust the temperature of the oil bath to 83 °C to keep the test solution in a slightly boiling state; (2) The experiment takes 48 hours as a cycle. After each cycle, the sample is taken out, and the black product on the surface of the material is brushed off with a soft brush in the running water. Wash and dry, for a total of 3 cycles; (3) Observe the surface of the corroded sample, and then observe it under a DM-IRM metallurgical microscope.

2.2.2. Shallow corrosion experiment

To determine the cause of intergranular corrosion, a shallow corrosion experiment is designed in this paper. The surface of the divided small sample was polished and then corroded with ferric chloride hydrochloric acid solution (ferric chloride 5 g + hydrochloric acid 50 ml + alcohol 100 ml) [8]. When the surface of the sample becomes gray-black, immediately wash off the etching solution with absolute ethanol, and then blow dry. Use SEM and Energy Dispersive Spectrometer (EDS) and other characterization methods to observe the corrosion morphology.

Due to the long etching time, the material that caused intergranular corrosion was completely corroded by the etching solution. To determine the substance of the corrosion ditch before corrosion, based on the original experiment, the etching time was shortened. When there is graying on the surface of the sample, the corrosion is over. Before the etching solution is completely etched away, the etching process is ended, so that the original substance can be retained on the surface of the substrate. At the same time, due to the action of the etching solution, the location of the etching material can be observed under SEM. The sample was cut longitudinally with a wire cutting machine, and the cut surface was ground and polished. The sample obtained is shown in Fig. 1. As shown in Fig. 1, in the obtained polished sample, the surface layer has a corrosion layer about several microns thick. There are two morphological features on the surface of the corrosion layer, the corrosion pits formed after corrosion and the substrate that is not sensitive to the etching solution. In the corrosion pit, part of

the specimen that has not been corroded remains on the surface of the specimen, and then the corrosion edge of the specimen longitudinally polished is scanned by EDS.

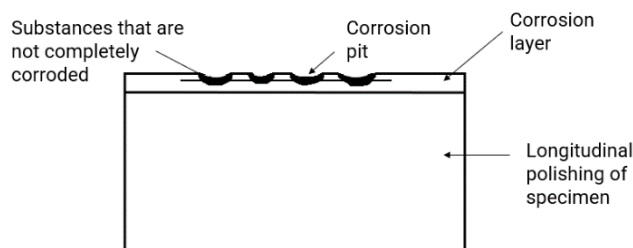


Fig. 1. Schematic diagram of the longitudinal polishing of the sample

3. RESULTS AND DISCUSSION

3.1. Fracture morphology

The appearance and morphology of the tensile fracture of the sample are shown in Fig. 2. The macroscopic appearance of the fracture is flat. There is obvious plastic deformation near the fracture of the specimen. The shape of the fracture is necked, the maximum shear stress in the fracture direction is parallel, and the angle of 45° with the principal stress direction can be judged to be plastic fracture [9].



Fig. 2. Fracture morphology of tensile specimen of 0Cr19Ni9 test steel

Fig. 3 shows the microscopic morphology of the tensile sample observed under the SEM. It can be seen from Fig. 3 that there are a large number of dimples in the sample, almost all of which are shear dimples. Except for the existence of dimples, fatigue bands are also distributed in them. After the macroscopic and microstructure observation of the tensile specimen, it is judged that the fracture is a plastic fracture [10]. Studies have shown that 0Cr19Ni9 steel is an austenitic stainless steel, which has excellent plastic toughness and also exhibits good plastic toughness during the stretching process [11]. Fig. 4 shows the tensile stress-

strain curve. According to Fig. 4, the plasticity and toughness of the samples are all excellent. The actual observed phenomenon also confirms this argument.

By observing the macroscopic and microscopic morphology, it can be determined that the blade has good plasticity and toughness, and the fracture is plastic fracture. It shows that the blade cracks are not caused by external factors. It is because of some changes in the internal organization during long-term operation that the local performance of the organization is weakened, leading to the initiation of the crack source. Coupled with the effect of long-term lateral stress, the crack source is expanded, which leads to the occurrence of cracks.

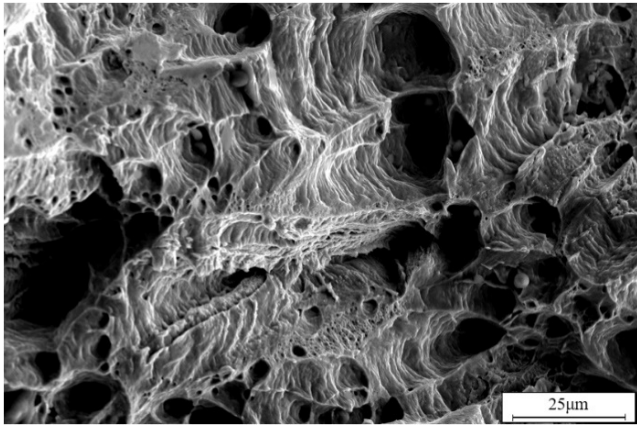


Fig. 3. Microscopic morphology of the tensile specimen

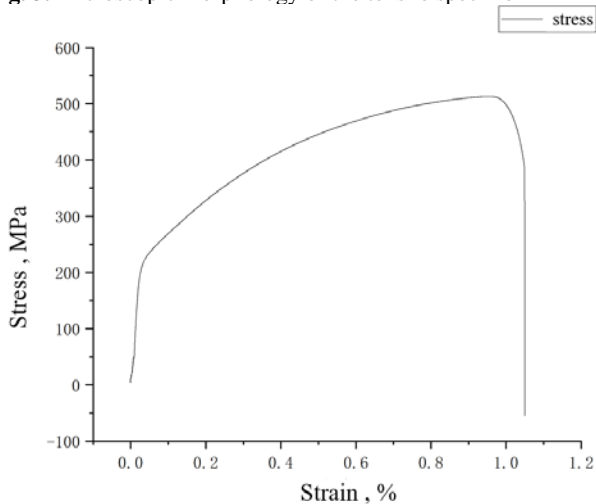


Fig. 4. Tensile stress-strain curve of 0Cr19Ni9

3.2. Intergranular corrosion appearance

Fig. 5 shows the corroded surface of a standard test specimen of GB/T 4334-2008 intergranular corrosion. The surface of the sample is gray-black as a whole, with knife-like corrosion. It is judged that there is a tendency of intergranular corrosion, but further observation by metallographic method is still needed.

The metallographic microstructure of 0Cr19Ni9 steel is corroded for 144 h in a slightly boiling state in the nitric acid solution, as shown in Fig. 6. It can be seen that there is a gray-black morphology, in which the gray-black matrix is austenite, and the black strips are the corrosion pits left after carbide corrosion. They are distributed in discontinuous bands between the austenite crystals, and the metallographic

structure is microscopic. The structure is characterized by obvious intergranular corrosion structure.



Fig. 5. Standard macro morphology of intergranular corrosion

In Cr-Ni stainless steel, if the steel is operated at a temperature of 450 ~ 850°C, or artificial aging treatment is carried out at this temperature, the intergranular corrosion tendency of the material will be greatly increased, which is called sensitization treatment [12, 13]. The working environment of the blade is 537 °C, 17.5 MPa, which is within the sensitization temperature range, and the susceptibility to intergranular corrosion is greatly increased. Through the macroscopic and microscopic observation of the sample surface, it can be judged that the blade has intergranular corrosion during operation.

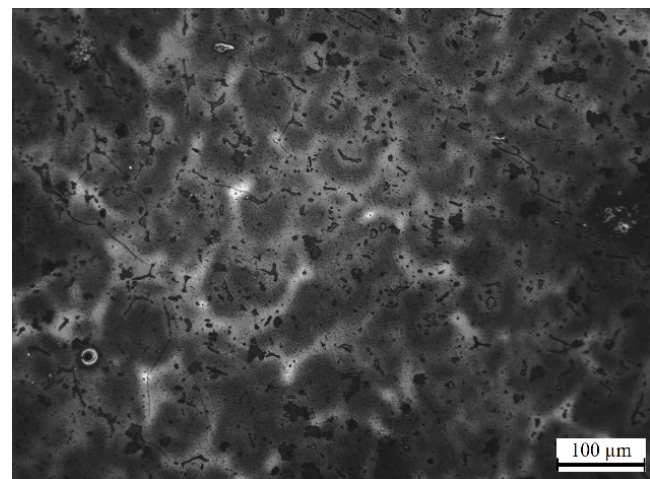


Fig. 6. Corrosion 144 h metallographic microstructure in the slightly boiling state of nitric acid

3.3. Analysis of shallow corrosion appearance

SEM was used to observe the surface of the first corroded sample as shown in Fig. 7. ①~⑥ representing the points where the EDS line spectrum fluctuates.

It can be seen from Fig. 7 that at ①④⑥, the radiation peaks intensity of Fe, Cr, and C drop sharply, and there is no increase in the radiation peaks of other elements, indicating that this is due to the pits formed after corrosion. At ②, the radiation peaks intensity of Si and Mn increase sharply, and are in a certain ratio, indicating that this is a Si-Mn metal compound. At ③, the radiation peaks intensity of Fe, Cr, Ni and C drop sharply, and the radiation peaks intensity of Si and Mn increase slightly, indicating that the pits formed after etching here expose the Si-Mn metal compound under the pits. At ⑤, the radiation peaks intensity of Fe and Cr drop

sharply, and at the same time, the radiation peak intensity of C increases. The author suspects that it is a pit formed after the chromium-rich area was corroded by the etching solution.

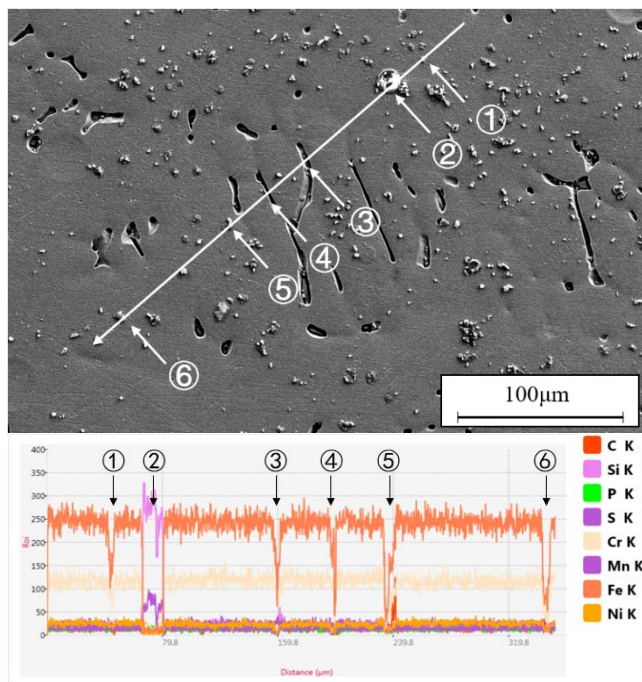


Fig. 7. 0Cr19Ni9 microstructure morphology

Based on the original corrosion experiment, the corrosion time is shortened. The observation under SEM is shown in Fig. 8. After reasonable corrosion, it can be observed that there is a concave area on the surface of the sample, which is a shallow corrosion area. Compared with the completely corroded area, in the shallow corroded area, only part of the material that caused the intergranular corrosion was corroded by the etching solution, and part of the material remained on the surface of the sample. The material composition can be detected by EDS. Fig. 9 shows the EDS scan result of the longitudinal edge of the sample. The scan result shows that there are carbides in ① and ②. At ①, the carbon content rises sharply, and the content of Fe and Cr drops sharply. There is precipitation of $Cr_{23}C_6$ [14, 15]. Cr should be enriched here, resulting in the surrounding Cr content being lower than that of the matrix. The Cr is more sensitive to the etching solution, but the C is less sensitive to the etching solution. Therefore, when $Cr_{23}C_6$ is corroded away, the Cr is separated from the substrate with the etching solution, and C remains on the surface of the substrate, causing the Cr content to continue to decrease here, while the C content exceeds the normal value. At ②, the content of C rises sharply, the content of Fe continues to decrease, and the content of Cr decreases slightly, which also proves the above. Due to the short corrosion time of the etching solution, some carbides are corroded, but there are still some carbides left on the surface of the substrate. The sharp increase in C content is due to the precipitation of C here. C combines with the surrounding Cr atoms to form $Cr_{23}C_6$ type carbides.

The etching solution corrodes some of the carbides, resulting in a decrease in the Cr content. At the same time, Cr content around ② is also lower than the surrounding value, which can also indicate that Cr atoms are enriched

here, forming a chromium-rich zone, and the surrounding is a chromium-poor zone [16]. It further proves that the test steel has a tendency of intergranular corrosion.

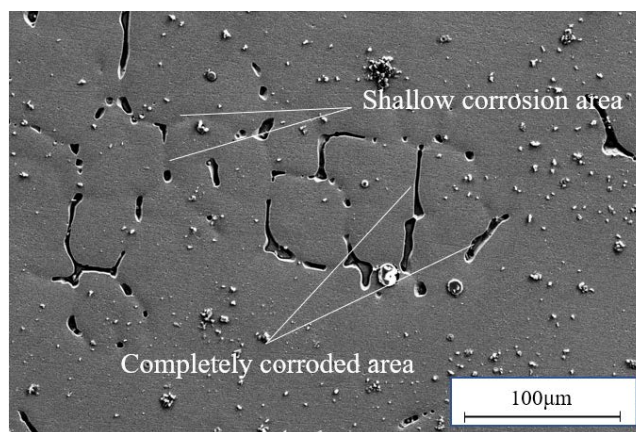


Fig. 8. 0Cr19Ni9 surface appearance of shallow corrosion

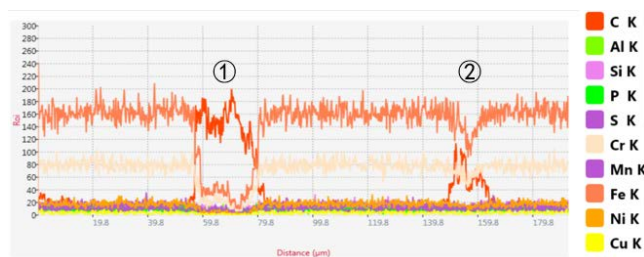
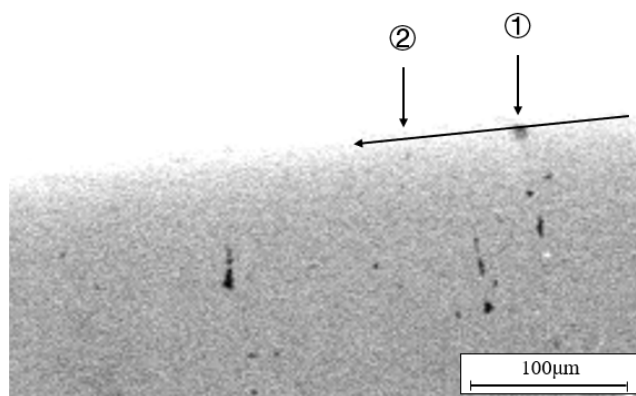


Fig. 9. 0Cr19Ni9 EDS scanning of longitudinal polishing edge

3.4. Discussion

Fig. 10 is a schematic diagram of the evolution of stainless steel intergranular corrosion. The original structure of 0Cr19Ni9 steel is almost 100 % austenite. Due to the high carbon content of the material, all C cannot be dissolved in the austenite. After solution treatment at 1050 °C for 2 h, the excess C can be dissolved in austenite to form a supersaturated solid solution, but the austenite at this time is a metastable phase. If the sample is heated at 400 ~ 850 °C, C will precipitate from the supersaturated γ -Fe solid solution, and rapidly diffuse to the grain boundaries and form precipitated phases with Cr, and precipitate on the grain boundaries to form a network of isolated protrusions. These phases are mainly Cr carbides. The movement rate of Cr in austenitic stainless steel is relatively slow, and it cannot move quickly from the inside of the crystal grain to the part where the Cr content is reduced.

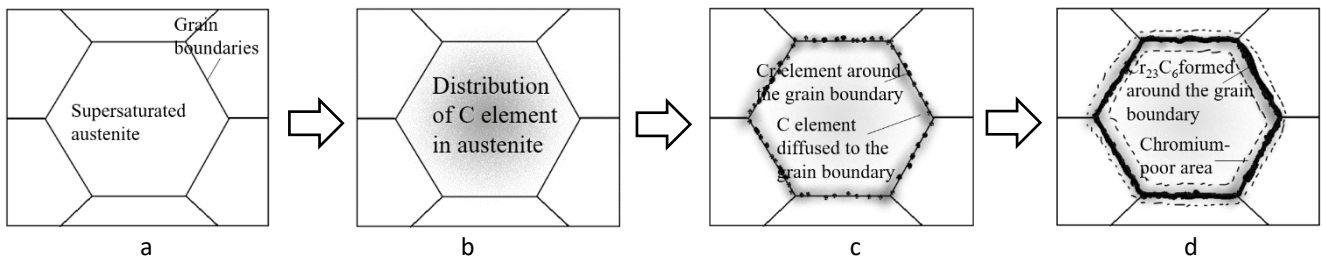


Fig. 10. Demonstration diagram of intergranular corrosion evolution: a–original organization; b–solution treatment; c–C element diffusion; d– Cr_{23}C_6 formation

This causes the Cr content in local areas to be lower than the content of the matrix for a long time, and the grain boundaries are plated with gold to form chromium-poor areas [17]. Since the electrode potential of Cr is higher than that of the austenitic stainless steel, the accumulation of Cr will cause differences in electrode potentials in local areas. When the material is in a corrosive medium, due to the difference in electrode potential of the material, it will lead to differences in the corrosion rate of different parts. Specifically, the corrosion rate near the grain boundaries is higher than that inside the grains, resulting in intergranular corrosion.

The carbon content of 0Cr19Ni9 steel is 0.054 wt.%, and the C content is relatively high, which induces obvious segregation of components [18]. The area with large C cannot be completely dissolved in austenite. When working within the sensitization temperature of intergranular corrosion, a large amount of C atoms are precipitated from the supersaturated γ -Fe solid solution. Because C can be closely combined with the surrounding alloy elements. When it meets the surrounding Cr, they will form many different types of carbides. According to the results calculated by JMatPro, we can see that the main carbide is Cr_{23}C_6 , and no other types of carbides are produced, as shown in Fig. 11.

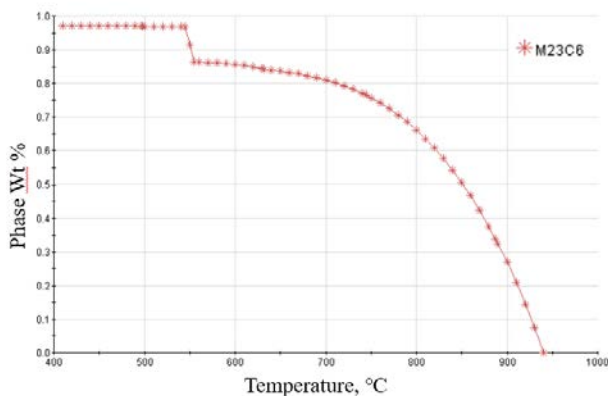


Fig. 11. Computational simulation of carbide precipitation by JMatPro

According to the precipitation kinetics of the M_{23}C_6 type carbide in 0Cr19Ni9 steel, these carbides mainly precipitate out in the grain boundary. Because the diffusion rate of Cr is very slow, the nearby Cr decreases, the local Cr content increases, and chromium-rich and chromium-depleted regions appear in the austenite matrix. Because electrode potential of Cr is high, the amount of Cr in the chromium-rich zone is higher than that of the matrix. The electrode potential of the chromium-rich zone is increased

and higher than that of the matrix. Because a large amount of Cr is enriched in the chromium-rich area, the Cr content of the matrix is much lower than that of the chromium-rich area, and the electrode potential decreases, which causes the electrode potential difference between the chromium-rich area and the matrix to increase. This leads to different electrode potentials of the same metal material in different areas on the microscopic level, forming a "big cathode" and "small anode" microbattery function.

The existence of this kind of micro-battery greatly reduces the corrosion resistance of austenitic stainless steel. The generation of intergranular corrosion not only leads to the decline of 0Cr19Ni9 corrosion resistance, but also destroys the continuity and stability of the material. As a result, various parts of the matrix material have different resistance to deformation, and their mechanical properties exhibit inconsistent plasticity and toughness. During the operation of the blade, the blade is subjected to transverse stress for a long time. The part with poor plasticity and toughness of the matrix is the part where the local damage of the material occurs preferentially. This is the reason why the intergranular corrosion causes cracks.

3.5. Improvement project

In production activities, the working environment of the blade cannot be changed, so it can only be improved from internal factors. This article points out that the occurrence of intergranular corrosion leads to the germination of crack sources. The content of C has a great influence on the susceptibility of the material to intergranular corrosion. With a small increase in the C content, the susceptibility of the material to intergranular corrosion will be greatly increased. Therefore, in the process of preparing the material, the C content should be appropriately reduced within the range allowed by the grade, which can effectively reduce the generation of intergranular corrosion. In addition, strong carbide formation elements like Ti and Nb are added to form stable TiC or NbC. It can stabilize the structure and prevent the formation of Cr_{23}C_6 and the generation of chromium-depleted areas, thereby improving the tendency to remove intergranular corrosion [19]. In order to achieve the purpose of eliminating intergranular corrosion, the amounts of Ti and Nb added to the steel are respectively: $0.8\% \geq \text{Ti} \geq 5\%$, $1\% \geq \text{Nb} \geq 10\%$ [20].

4. CONCLUSIONS

Through the observation of fracture morphology, the standard experiment of intergranular corrosion and the verification and analysis of shallow corrosion experiment, it was determined that the intergranular corrosion caused

blade cracks and the products of intergranular corrosion were determined: (1) According to the tensile stress-strain curve, the sample has excellent plastic toughness. And judging from the fracture morphology, it is concluded that the sample is plastic fracture; (2) In the standard test of intergranular corrosion and shallow corrosion test, it can be seen that the cause of blade cracks is long-term service causes the C and Cr to undergo a diffusion reaction to form Cr-rich areas and carbides, which are easy to be thermally corroded in the service environment. The Cr-rich areas are reduced and the strength of the area is reduced. The carbides accumulate at the grain boundary, causing groove-like defects to form at the grain boundary, which produces a cutting effect and is easy to form a source of fatigue cracks.

Acknowledgments

This research was Supported by National Defense Key Laboratory Fund(No. 6142909200106).

REFERENCES

- Zhang, X.L., Wang, W.M.** Five Dimensional Movement Measurement Method for Rotating Blade Based on Blade Tip Timing Measuring Point Position Tracking *Mechanical System and Signal Processing* 161 2021: pp. 107898. <https://doi.org/10.1016/j.ymssp.2021.107898>
- Wu, M.S., Zhao, Y.Z.** The Analysis and Solution of Contact Rubbing Fault for Low Pressure Rotor of Gas-steam Combined Cycle Turbine Unit *IOP Conference Series: Earth and Environmental Science* 446 2020: pp. 022078. <https://doi.org/10.1088/1755-1315/446/2/022078>
- Lin, A.Q., Chang, X.Y.** Effect of Wet Steam on Aerodynamic Performance of Low-Pressure Exhaust Passage with Last Stage Blade *Journal of Applied Fluid Mechanics* 12 (6) 2019: pp. 1837–1845. <https://doi.org/10.29252/jafm.12.06.29757>
- Zheng, M.B., Chen, G.H.** Failure Analysis on Two Austenitic Stainless Steels Applied in Cyclone Separators of Catalytic Cracking Unit *Engineering Failure Analysis* 2010: pp. 88–96. <https://doi.org/10.1016/j.engfailanal.2010.08.008>
- Shen, L.J., Ma, Y.L.** The Morphology and Content of Delta Ferrite in Non-Equilibrium Solidified 0Cr18Ni9 Austenitic Stainless Steel *Advanced Engineering Materials II* 2012: pp. 666–669. <https://doi.org/10.4028/www.scientific.net/AMR.535-537.666>
- Luo, W.** Effect of Micro-plasma arc Melting on the Corrosion Resistance of a 0Cr19Ni9 Stainless Steel SAW Joint *Material Letters* 55 (5) 2002: pp. 290–295. [https://doi.org/10.1016/S0167-577X\(02\)00380-4](https://doi.org/10.1016/S0167-577X(02)00380-4)
- GB/T 4334-2008, Corrosion of Metals and Alloys - Stainless Steel Intergranular Corrosion Test Method *The General Administration of Quality Supervision, Inspection and Quarantine of the People's Republic of China and the National Standardization Administration of the People's Republic of China*, 2008.
- Wang, S.F., Ding, F.** Study on Reducing Side Etching of Copper Microelectrode by Multi-Step Etching Process *Materials Research Express* 12 (6) 2019: pp. 126411. <https://doi.org/10.1088/2053-1591/ab583d>
- Fan, T.Y.** Plastic Fracture of Quasicrystals *Philosophical Magazine* 2008: pp. 523–535. <https://doi.org/10.1080/14786430801894536>
- Tanabe, Y.** Fracture Toughness for Brittle Fracture of Elastic and Plastic Materials *Material Transaction* 54 (3) 2013: pp. 314–318. <https://doi.org/10.2320/matertrans.M2012348>
- Xie, J.B., Fan, T., Fu, J.X.** Enhancement of Impurity, Machinability and Mechanical Properties in Te-treated 0Cr18Ni9 Steel *Metals and Materials International* 27 (6) 2021: pp. 1416–1427. <https://doi.org/10.1007/s12540-019-00545-3>
- José, C.L.** Comparative Study Between Sensitization Degree of the 0.4% Mo Austenitic Stainless Steel and UNS S31803 Duplex Stainless Steel *Materials Research-Iberia-American Journal of Materials* 24 (1) 2020. <https://doi.org/10.1590/1980-5373-MR-2020-0408>
- Wasnik, D.N.** Controlling Grain Boundary Energy to Make Austenitic Stainless Steels Resistant to Intergranular Stress Corrosion Cracking *Journal of Materials Engineering and Performance* 2003: pp. 402–407. <https://doi.org/10.1361/105994903770342926>
- Huang, C.F.** Research of Phase Transformation on Fe-8.7Al-28.3Mn-1C-5.5Cr Alloy *Journal of Alloys and Compounds* 2009: pp. 246–249. <https://doi.org/10.1016/j.jallcom.2009.08.097>
- Anindya, G.** Structural and Electronic Properties of Chromium Carbides and Fe-Substituted Chromium Carbides *Materials Research Express* 2020: pp. 056508. <https://doi.org/10.1088/2053-1591/ab8cf9>
- Kim, H.P.** Intergranular Corrosion of Stainless Steel *Corrosion Science and Technology-South Korea* 2018: pp. 183–192. <https://doi.org/10.14773/cst.2018.17.4.183>
- Luo, W.** The Corrosion Resistance of 0Cr19Ni9 Stainless Steel Arc Welding Joints with and without Arc Surface Melting *Materials Science and Engineering A345* 2002: pp. 1–7. [https://doi.org/10.1016/S0921-5093\(02\)00397-0](https://doi.org/10.1016/S0921-5093(02)00397-0)
- Li, H.** Effect of Heat Treatment on the Microstructure and Corrosion Resistance of Stainless/Carbon Steel Bimetal Plate *Progress in Materials Science and Engineering* 2020: pp. 1280761. <https://doi.org/10.1155/2020/1280761>
- Kim, J.M., Lee, H.W.** Study for Corrosion Characteristics of Ferritic Stainless Steel Weld Metal with Respect to Added Contents of Ti and Nb *Metals and Materials International* 2014: pp. 329–335. <https://doi.org/10.1007/s12540-014-1019-8>
- Kim, S., Jang, S.K.** Effects of Alloy Elements on Electrochemical Characteristics Improvement of Stainless Steel in Sea Water *Journal of Advanced Marine Engineering and Technology* 2014: pp. 890–899. <https://doi.org/10.5916/jkosme.2014.38.7.89>



© Li et al. 2022 Open Access This article is distributed under the terms of the Creative Commons Attribution 4.0 International License (<http://creativecommons.org/licenses/by/4.0/>), which permits unrestricted use, distribution, and reproduction in any medium, provided you give appropriate credit to the original author(s) and the source, provide a link to the Creative Commons license, and indicate if changes were made.